JOURNAL OF MATERIALS SCIENCE 15 (1980) 1131–1139

The crystallization of the amorphous alloy $Fe_{40}Ni_{40}P_{14}B_6$

TOHRU WATANABE*, MICHAEL SCOTT
University of Sussex, School of Engineering and Applied Sciences, Brighton, Sussex, UK

The isothermal transformation behaviour of the metallic glass $Fe_{40}Ni_{40}P_{14}B_6$ between 320 and 400° C is described. Crystallization occurs by a eutectic mechanism to form Fe–Ni austenite and a body-centred tetragonal phase which is isomorphous with Fe_3P and Ni_3P. The eutectic crystals have a barrel shape such that the *c*-axis of the tetragonal phase is parallel to the barrel axis. The orientation relationship between the two phases is $\langle 1\,1\,0\rangle T \parallel \langle 1\,1\,0\rangle_\gamma$ and $\langle 0\,0\,1\rangle T \parallel \langle 1\,1\,2\rangle_\gamma$. The austenite phase contains (1 1 1) twins.

1. Introduction

Since their discovery nearly 20 years ago [1] metallic glasses have developed from a scientifically interesting phenomenon to technologically useful materials. Their properties have been the subject of a number of recent reviews [2, 3]. In their as-quenched state metallic glasses are metastable and consequently on subsequent annealing they undergo a number of structural changes [4]. At relatively low temperatures and short times, densification [5] and short range ordering occur [6], accompanied by changes in magnetic anisotropy, Curie temperature, modulus, ductility and specific heat [7–9]. At temperatures near the glass transition temperature crystallization occurs. It is well established that the crystallization mechanism is the nucleation and growth of discrete crystals within the glassy matrix with transformation kinetics similar to those for crystal growth from metallic melts [4]. Frequently the crystals which form are not those of the equilibrium phase in the alloy.

One of the most thoroughly investigated glassy metallic alloys is $Fe_{40}Ni_{40}P_{14}B_6$, mainly on account of its easy commercial availability as Metglas 2826 from Allied Chemical Corporation. The thermal stability of this particular alloy has been the subject of a number of investigations. Scott [10] has shown that the crystallization kinetics as measured by differential scanning calorimetry can be fitted by the Johnson–Mehl–Avrami equation with an exponent of 4. Measurements of various physical properties have confirmed that the time for onset of crystallization has an Arrhenius dependence on temperature with an activation energy of about 400 kJ mol^{-1} [10–12]. In a microstructural investigation Walter *et al.* [13] claimed that the partially transformed material contained highly twinned crystals of a body-centred tetragonal phase isomorphous with Fe_3P. However, they were unable to identify unambiguously the fine structure within the crystals. In the present paper the isothermal transformation diagram for the alloy is presented. The morphology and crystallography of the glass-to-crystal transformation are described in detail and in particular it is shown that, contrary to the interpretation of Walter *et al.* [13], decomposition of the glass occurs by a eutectic-type reaction to give austenite and a tetragonal phase. A well-defined crystallographic orientation relationship exists between the two phases.

2. Experimental details

The $Fe_{40}Ni_{40}P_{14}B_6$ glass was supplied by Allied Chemical Corporation in the form of ribbon 2 mm wide and approximately 50 μm thick. Isothermal heat treatments were carried out

*Permanent address: Tokyo Metropolitan University, Department of Industrial Chemistry, 2-1-1 Fukazaura, Setagaya, Tokyo, Japan.

0022–2461/80/051131–09$02.90/0

between 325 and 400° C by sealing 50 mm lengths of the ribbons in evacuated quartz tubes and annealing in a small tube furnace with a long hot zone (120 mm). Temperature control was within ± 0.5° C. For optical and scanning electron microscopy the ribbons were electroplated with approximately 50 μm nickel, mounted transversely in 0.2 mm slots in a stainless steel block and immersed in cold setting resin. After conventional metallographic preparation the polished specimens were etched in acidic ferric chloride. Specimens were prepared for transmission electron microscopy by jet polishing with an electrolyte of 80% ethanol, 20% perchloric acid at −40° C and a current density of approximately 2×10^{-4} A mm^{-2}. They were examined at 120 kV in a JEOL 120C microscope. Microdiffraction and microanalysis were performed using a JEOL TEMSCAN system with energy dispersive X-ray analysis facilities. X-ray diffraction information was obtained by powder photography and scanning diffractometry using cobalt radiation.

3. Results and discussion

The glassiness of the as-received material was confirmed by electron microscopy. All specimens gave a diffraction pattern which consisted of two broad haloes and the accompanying bright-field micrographs were featureless. After isothermal annealing, the specimens contained a uniform distribution of "spherulitic" crystals as shown in Fig. 1. These crystals, which at low annealing temperatures were as large as 10 μm, had a two-phase lamellar appearance which is discussed in detail below. Specimens annealed at 325° C contained, in addition, crystals of a different morphology, which is also described later. The sections of the spherulitic crystals ranged from circular to rectangular and, assuming a constant crystal shape, could all be described as suitable intersections of a plane with a barrel shape, as illustrated in Fig. 2. As would be expected for crystal growth in an isotropic amorphous medium there was no preferential orientation of the crystals with respect to the plane of the ribbon. From optical and scanning electron micrographs of transverse sections it was also apparent that the crystals nucleated uniformly throughout the ribbon cross-section (Fig. 3). This observation contradicts previous suggestions that compositional differences between the surface and bulk of the ribbons might lead to differences in crystallization rate [14]. Moreover, the behaviour of this glass differs from that of $Fe_{40}Ni_{40}B_{20}$ where crystal growth was from the ribbon surfaces and $Fe_{80}B_{20}$ where there was a precipitate-free zone near the specimen surface [15]. The crystals grew without apparent change of morphology until they impinged, confirming the suggestions

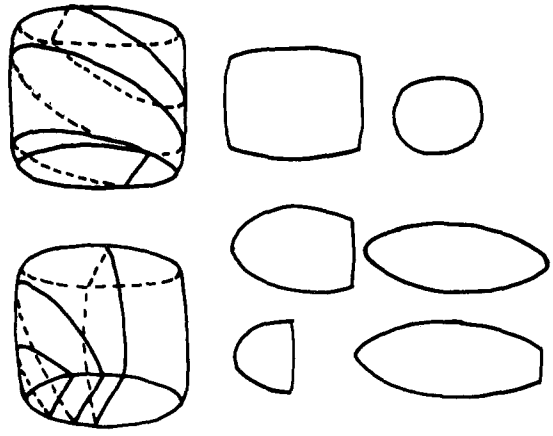

Figure 2 Schematic to show barrel shape of crystals and expected sections.

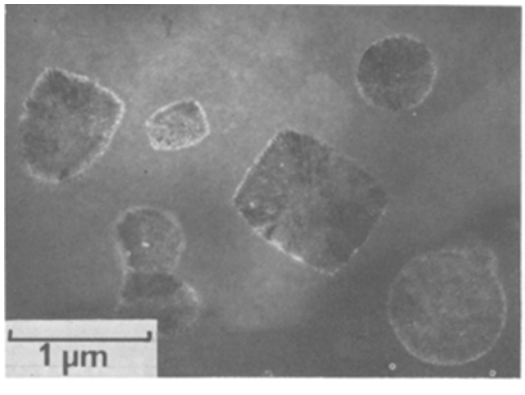

Figure 1 Typical distribution of crystals in specimen annealed 11 min at 385° C.

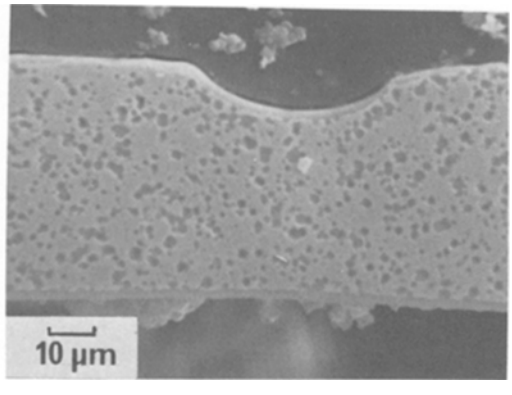

Figure 3 Scanning electron micrograph of ribbon cross-section annealed 3 h at 365° C.

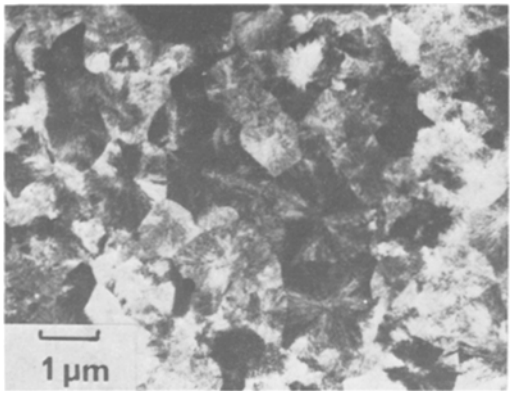

Figure 4 Fully transformed specimen, 20 min at 385° C.

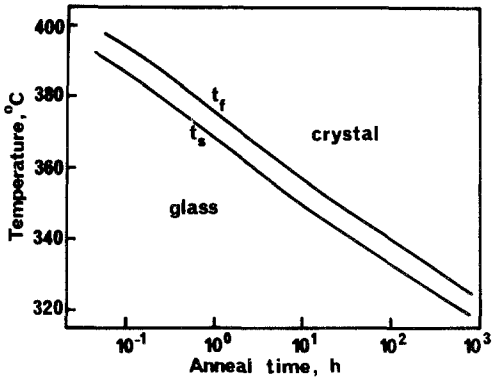

Figure 6 Isothermal transformation diagram for the glass $Fe_{40}Ni_{40}P_{14}B_6$. t_s and t_f are, respectively, the times for start and completion of crystallization.

from DSC work that the crystallization of this alloy occurs in a single stage [10]. The grain size of the fully transformed specimens (Fig. 4) was strongly temperature dependent ranging from less than 1 μm at 400° C to 8 μm at 330° C (Fig. 5).

The bright-field micrographs were used to construct the TTT diagram for the alloy shown in Fig. 6. The start and finish lines represent the annealing times and temperatures at which crystals were first detectable and at which complete impingement of the growing crystals had occurred. The crystallization start times (t_s) determined in this work were in good agreement with those determined previously by differential scanning calorimetry [10] and magnetic measurement [11]. t_s showed an Arrhenius dependence on absolute temperature over the whole temperature range investigated with an activation energy of $4.3 \pm 0.1 \times 10^5$ J mol^{-1} (Fig. 7). This value is approximately 10% larger than that determined previously for the same alloy [10–12]. Such discrepancies probably arise from the relative sensitivities of the difference experimental techniques to small percentages of crystallinity. In order to study the kinetics of the transformation, estimates of the volume fraction transformed were made by area measurements on the bright-field micrographs. When plotted against time, t, the fraction transformed $z(t)$ had the sinusoidal shape characteristic of nucleation and growth reactions. According to standard nucleation and growth kinetics, $z(t)$ should be related to t by [16]:

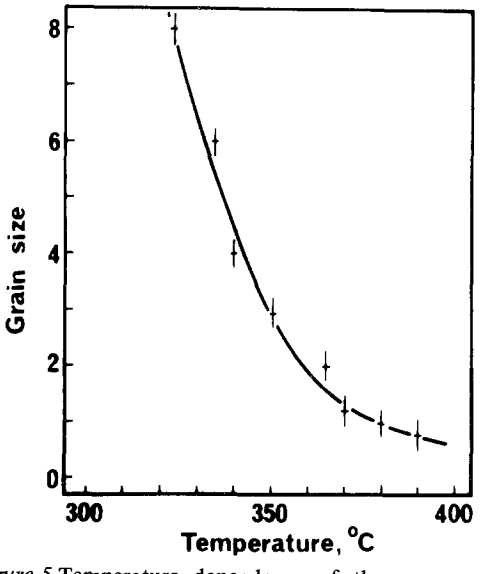

Figure 5 Temperature dependence of the average grain size of fully transformed specimens.

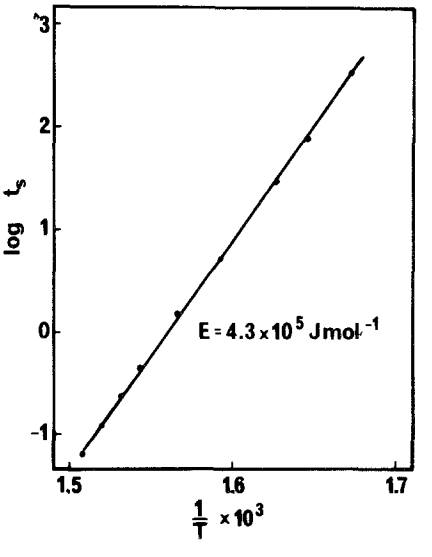

Figure 7 Temperature dependence of onset time for crystallization.

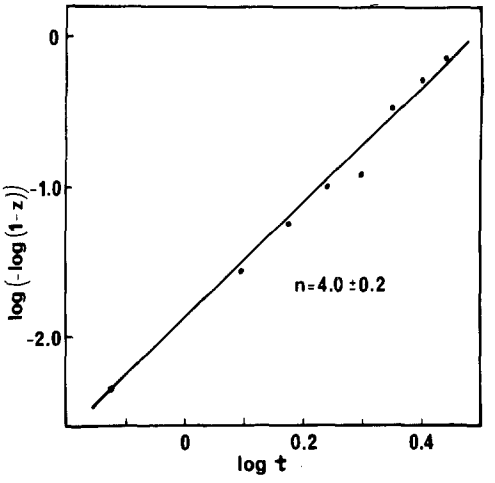

Figure 8 Fit of $z(t)$ for specimens annealed at 365° C to Johnson–Mehl–Avrami equation.

$$z(t) = 1 - \exp(-kt^n)$$

where $t = 0$ is taken as the end of the incubation period. In its logarithmic form the above equation becomes

$$\log(-\log(1-z)) = n \log t + \text{const.}$$

Fig. 8 shows a plot of the data obtained from isothermal annealing at 365° C. Within experimental limits a linear plot is obtained with the exponent $n = 4.0 \pm 0.2$, in agreement with results obtained on the same alloy by differential scanning calorimetry [10]. According to standard theory of phase transformations, an exponent of $n = 4$ in the Johnson–Mehl–Avrami equation should arise from either a eutectoid or polymorphic transformation where the nucleation rate is constant [16, 17]. In both cases the reaction is of the discontinuous type, where the average composition of the product and that of the matrix are the same and therefore there is no long-range composition gradient ahead of the growing particles. With this in mind, microanalysis was performed on the partially crystallized specimens using a JEOL TEMSCAN system fitted with energy dispersive analysis facilities. Although no analysis was possible for boron it was possible to show that within experimental accuracy the ratio of the integrated counts for Fe$K\alpha$, Ni$K\alpha$ and P$K\alpha$ were the same in both the crystals and the amorphous matrix. Moreover, within the spatial resolution limits possible, the crystals were compositionally homogeneous. However, it should be noted that the internal structure of the crystals was on a scale finer than the smallest area that could be analysed.

X-ray diffraction patterns of fully transformed specimens at all annealing temperatures were identical. In all cases an f c c phase was clearly present with lattice parameter $a_0 = 0.357 \pm 0.002$ nm. In addition, there were a large number of other reflections of which the indexing is discussed later. The lattice parameter of the f c c phase is consistent with that for Fe–Ni austenite, although it is not possible to estimate the Fe : Ni ratio since the lattice parameter does not vary significantly with composition above 50 at% Fe [18]. No evidence was found in the X-ray diffraction patterns for the presence of α–Fe. Walter *et al.* [13] also suggested, on the basis of X-ray diffraction, that the crystallization products of amorphous $Fe_{40}Ni_{40}P_{14}B_6$ were austenite and a tetragonal phase together with a little ferrite. It is therefore suprising that in their electron micrographs they presented no evidence for the presence of austenite or ferrite. Instead they described their crystals as consisting of a single Fe_3P-type phase; in the early stages of growth the crystals were perfect but at later stages contained several twin orientations. In all cases there was a fine structure of "plates and spheroids", the exact nature of which was not specified. Fig. 9a shows a roughly circular cross-section of a crystal grown after 42 min at 372° C in the present work. Here the barrel axis is perpendicular to the plane of the foil. The crystal has a clear two-phase lamellar appearance, like that obtained during eutectic reactions and not dissimilar from that displayed by polymer spherulites. Towards the edge of the section the lamellae have a radial arrangement, whereas in the centre of the section it is clear that they are oriented in only two mutually perpendicular directions. The high magnification micrograph from the centre of the crystal section (Fig. 9b) shows this more clearly. The diffraction pattern from this section (Fig. 9c) is a simple square pattern. The closest spot to the origin corresponds to a lattice spacing of ~ 0.063 nm and if this is taken as (1 1 0), the diffraction pattern is consistent with an ⟨0 0 1⟩ orientation of the tetragonal phase proposed by Walter *et al.* [13] ($a_0 = 0.89$ nm). After correction for lens rotation it is seen that the lamellae in the centre of the crystal section lie parallel to ⟨1 1 0⟩ of the tetragonal phase. In an attempt to reconcile the apparent two-phase lamellar structure of the crystals with the apparently single-phase diffrac-

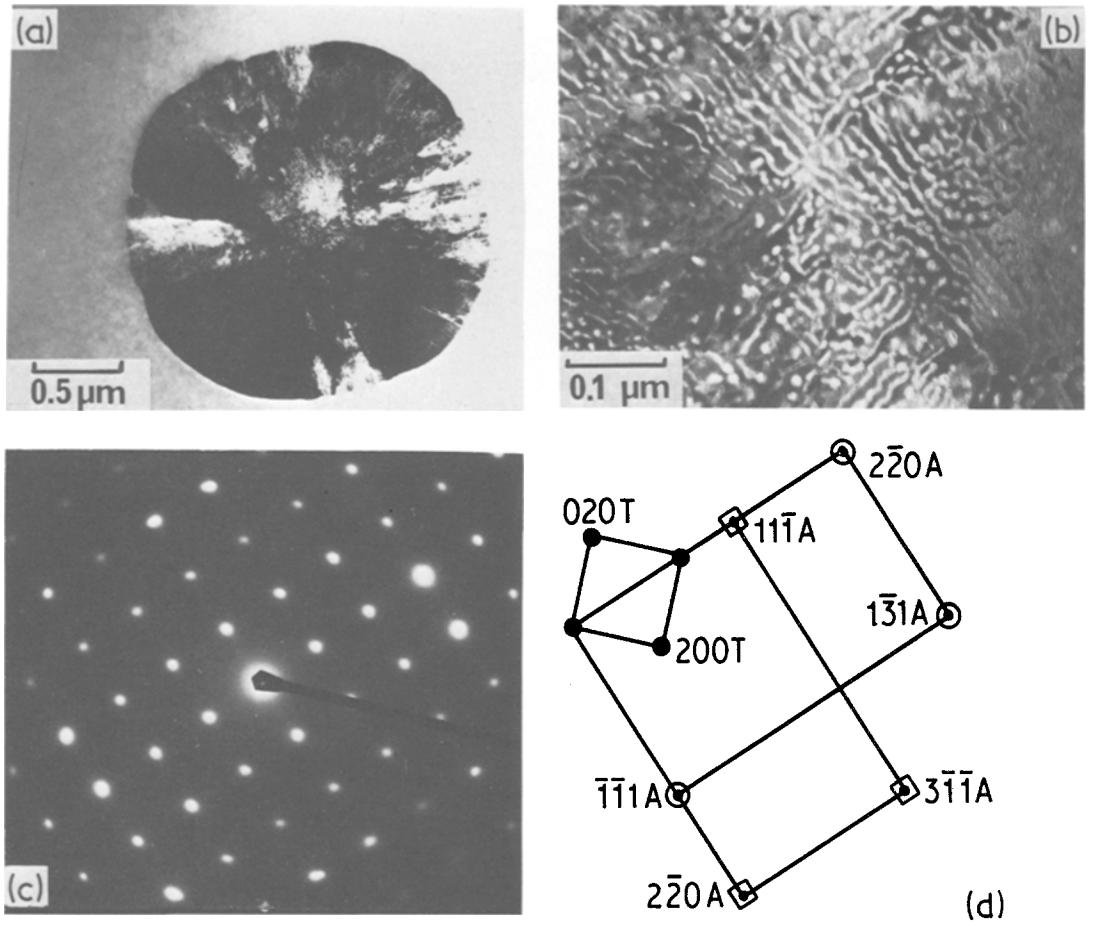

Figure 9 (a) Approximately circular ⟨0 0 1⟩T section of crystal, 42 min at 372° C. (b) High magnification image to show fine structure at centre of crystal. (c) Diffraction pattern from this section. (d) Indexing of the diffraction pattern (c). • tetragonal phase, ○□ γ-phase.

tion pattern, dark-field images were obtained in turn from each of the diffraction spots in Fig. 9c. The pertinent results are shown in Fig. 10 where the dark-field micrographs are labelled according to the diffraction spot from which they were obtained. For every spot in the pattern the matrix was illuminated. However, for only a few spots were the lamellae (light in the bright-field micrograph) illuminated. These were the spots which appeared brightest in the diffraction pattern, i.e. spots (b) and (d). The lattice spacing corresponding to these spots, i.e. 0.208 nm, is that expected from (1 1 1) of the f c c γ-phase identified by X-ray diffraction. Moreover, it should be noted that for each γ reflection only one orientation of the lamellae is illuminated in the dark-field micrograph. It was therefore concluded that the crystals were indeed two-phase; the matrix was the tetragonal phase, and the lamellae the austenite phase.

Two orientations of the austenite were present and the diffraction pattern of Fig. 9c consisted of an ⟨0 0 1⟩ tetragonal pattern with two superimposed ⟨1 1 2⟩ austenite patterns rotated 90° about $\langle 1\ 1\ 2\rangle_\gamma$ with respect to each other such that ⟨1 1 0⟩ austenite was parallel to ⟨1 1 0⟩ tetragonal. An annotated guide to indexing of the patterns is shown in Fig. 9d.

Fig. 11a shows a section through a crystal which is perpendicular to that discussed above such that it contains the axis of the barrel shape, ⟨0 0 1⟩ tetragonal, and one of the tetragonal ⟨1 1 0⟩ directions. The associated diffraction pattern is shown in Fig. 11c. Fig. 11d shows how this pattern can be indexed consistently with the deductions made above. This section of reciprocal space included two orientations of the austenite phase, i.e. a $[\bar{1}\ 1\ 0]$ and a $[1\ 1\ \bar{1}]$ section together with a $[\bar{1}\ 1\ 0]$ tetragonal section. The

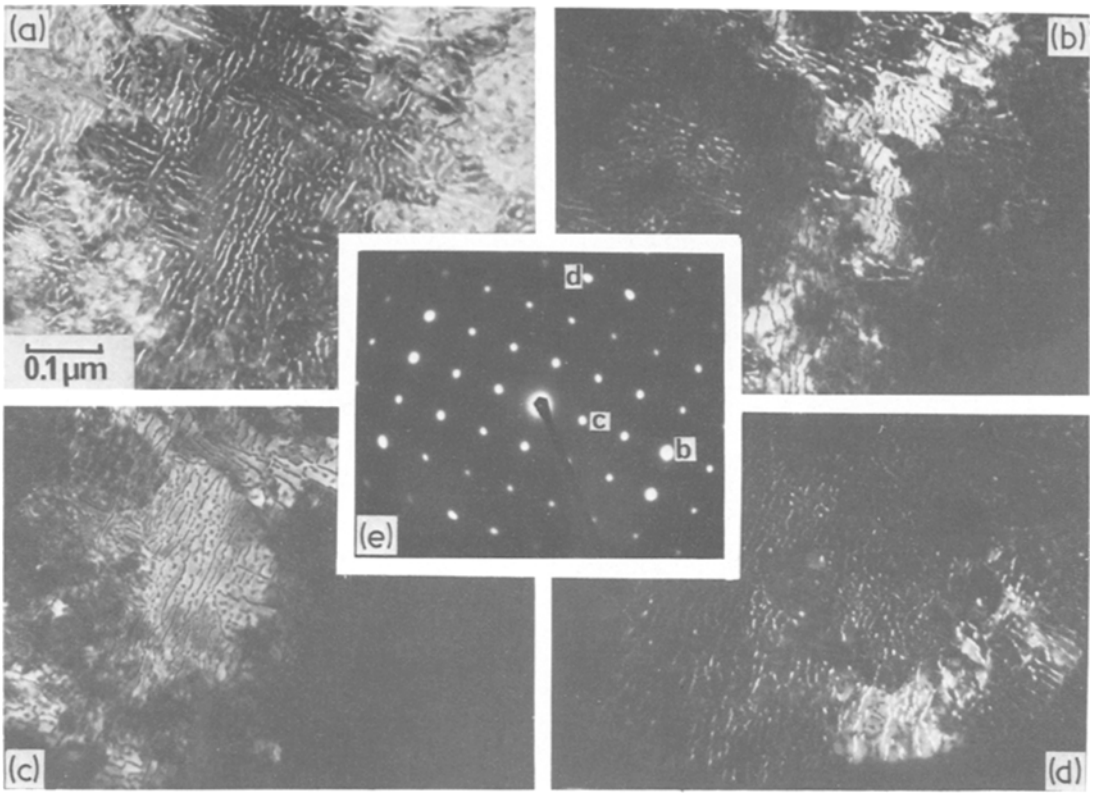

Figure 10 Dark-field images from ⟨0 0 1⟩T section. (a) the bright-field image. (b) to (d) Dark-field images from the spots marked in the diffraction pattern (e).

tetragonal phase is oriented such that [1 1 0]T is parallel to [1 $\bar{1}$ 0] austenite and the tetragonal c-axis is parallel to [1 1 2] of the austenite phase. If $(2\ 2\ 4)_\gamma$ and (0 0 6)T are taken as coincident, the c parameter of the tetragonal phase is approximately 0.44 nm, in agreement with that proposed by Walter *et al.* [13]. A number of reflections in the diffraction pattern of Fig. 11c cannot be explained on this basis. Since these reflections are absent in the X-ray diffraction patterns, it is assumed that they arise from double diffraction. This could easily be the case if for example the $(0\ 2\ 2)_\gamma$ reflection is subsequently diffracted by the tetragonal phase. One striking feature of the diffraction pattern in Fig. 11c is the well-defined streaking which in this and all other cases is perpendicular to the tetragonal c-axis. From the micrograph (Fig. 11a) it is clear that the streaking lies perpendicular to only one direction of the lamellae. Thus the streaking does not arise from the lamellae themselves but possibly from some fine structure within the lamellae. At high magnifications (Fig. 11b) it can be seen that the austenite phase contains fine structure in the form of fringes with a separation of about 5 nm. These fringes are perpendicular to the streaks in the diffraction pattern and therefore to ⟨1 1 1⟩ of the austenite. Hence it is suggested that the fringes arise from either stacking faults or microtwins within the f c c austenite. The presence of twins on the {1 1 1} f c c planes is included in the interpretation of the diffraction pattern (Fig. 11c and d). No extra spots are introduced. Walter *et al.* [13] have also proposed that twinning is present in the crystals, but within the tetragonal phase. They claimed that adjacent quadrants of the crystals had twin orientations with respect to each other. That this cannot be the case is shown in Fig. 12 where the diffraction patterns from two adjacent quadrants are identical. (To avoid overlap with adjacent quandrants it was necessary to include some of the amorphous matrix within the selected area which explains the presence of the halo in the diffraction patterns).

From the evidence presented above it was concluded that the amorphous phase decomposes by a eutectic type mechanism into austenite and a tetragonal phase. (The term eutectic is preferred

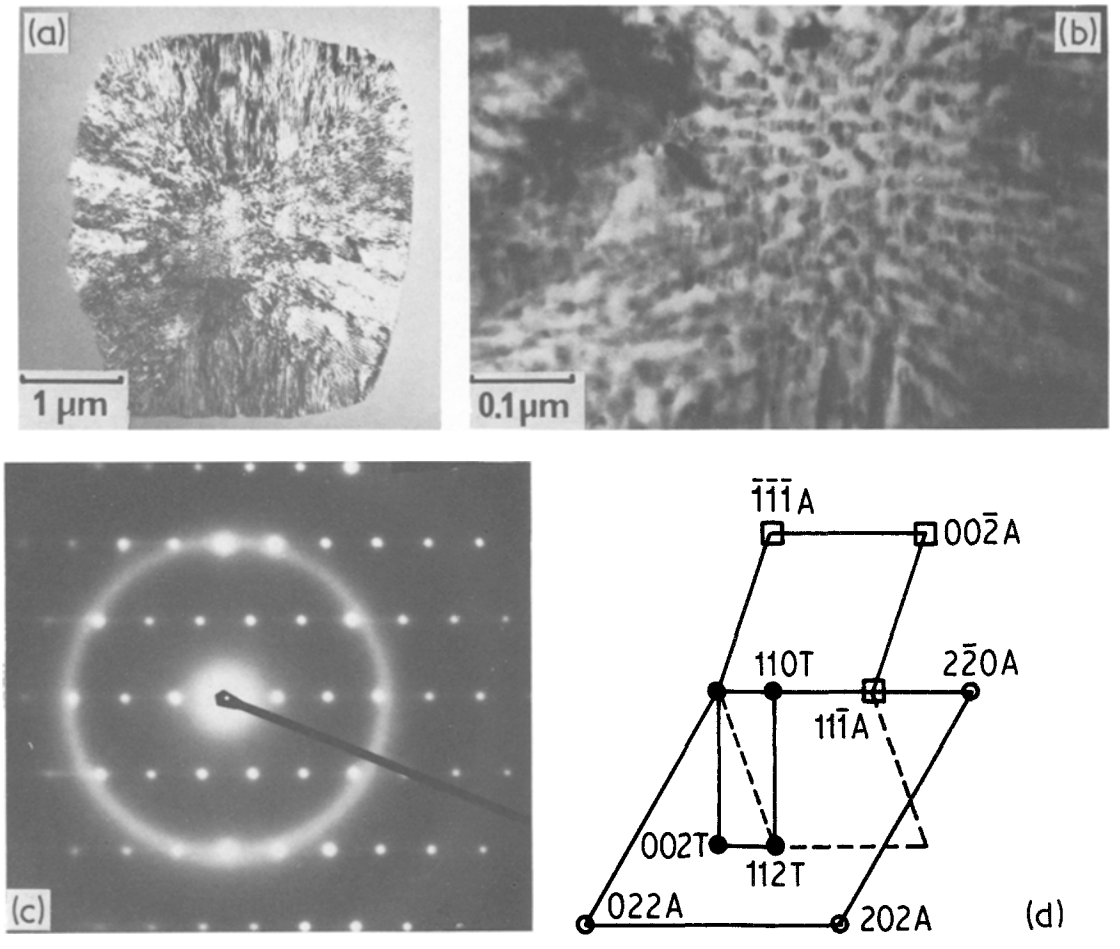

Figure 11 (a) Crystal section containing barrel axis, 11 h at 355° C. (b) High magnification of portion to show fringes. (c) Diffraction pattern from (a). (d) Indexing of the diffraction pattern in (c). • Tetragonal phase, ○□ γ-phase. The twinned reciprocal lattices are shown in dotted lines.

to eutectoid since although the reaction is occurring in the solid state the parent phase is essentially a highly undercooled liquid). The two phases grow in a coupled fashion such that:

⟨1 1 0⟩ tetragonal ‖ ⟨1 1 0⟩ austenite

⟨0 0 1⟩ tetragonal ‖ ⟨1 1 2⟩ austenite.

Similar eutectic decompositions have been observed in other amorphous metallic systems such as Fe–B [19] and Pd–Cu–Si [20]. In the case of $Fe_{80}B_{20}$, microstructures similar to those described here were found, with α–Fe platelets embedded in a matrix of a metastable iron boride. In the present work, unambiguous identification of the tetragonal phase is not possible. From the X-ray diffraction patterns the lattice parameters were determined as $a = 0.885$ nm $c = 0.440$ nm (both ± 0.005 nm) and the systematic absences characteristic of a body-centred lattice. The lattice parameters are similar to those for $(FeNi)_3P$ which has a body-centred tetragonal structure with $a = 0.901$ nm, $c = 0.447$ nm at an Fe:Ni ratio of 1 [18]. In addition, the phase Fe_3P can absorb boron up to $Fe_3P_{0.64}B_{0.36}$ [18] which is a higher boron content than in the present alloy. It is probable, therefore, that the tetragonal phase is of the type $(FeNi)_3(PB)$ isomorphous with Fe_3P and Ni_3P.

Finally it should be mentioned that the crystallization morphologies discussed in this paper apply only to alloys heat treated above about 330° C. Specimens annealed at 325° C, in general, did not show the barrel-shaped crystals obtained at higher temperatures. The crystals were of irregular shape and contained many subgrains (Fig. 13). Within these grains the same two-phase lamellar appearance

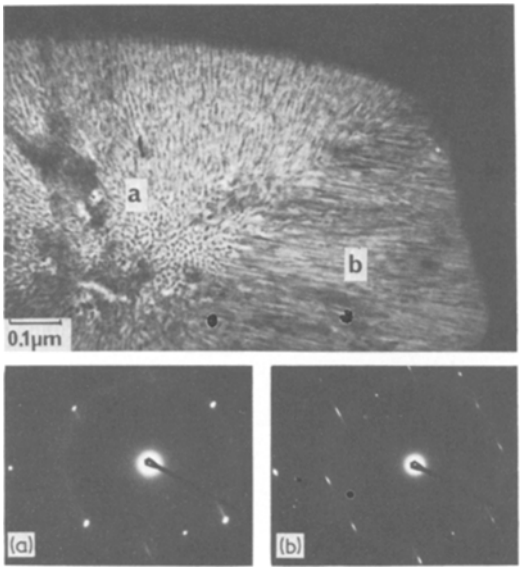

Figure 12 Diffraction patterns from adjacent "quadrants" of crystal, 11 h at 355° C.

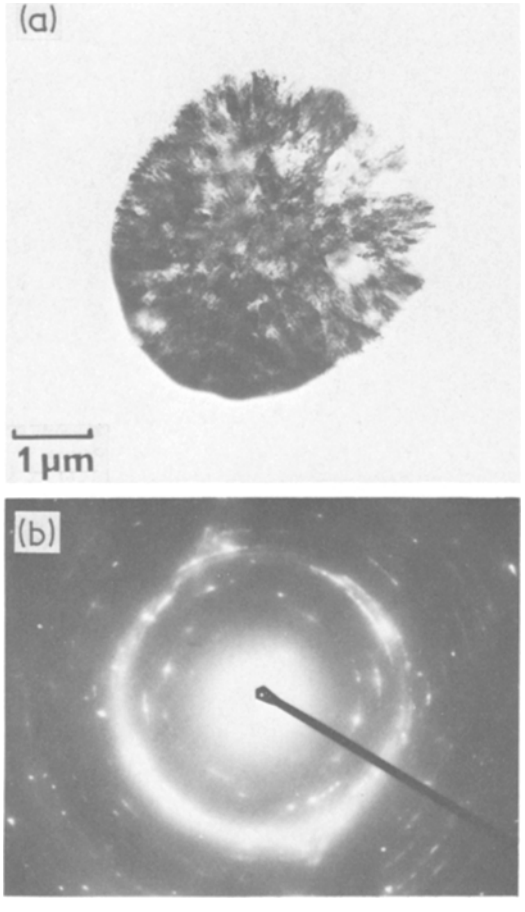

Figure 13 (a) Specimen annealed 400 h at 325° C. (b) Diffraction pattern from (a).

was still visible. Further analysis of these crystals has yet to be carried out.

4. Conclusions

The amorphous alloy $Fe_{40}Ni_{40}P_{14}B_6$ crystallizes by a eutectic mechanism to austenite and a body-centred tetragonal phase which is probably $(FeNi)_3(PB)$. The orientation relationship between the phases is

$$\langle 1\ 1\ 0\rangle T \parallel \langle 1\ 1\ 0\rangle_\gamma$$

$$\langle 0\ 0\ 1\rangle T \parallel \langle 1\ 1\ 2\rangle_\gamma.$$

The austenite phase is probably twinned on $\{1\ 1\ 1\}$ planes. The crystals have a well-defined barrel shape with $\langle 0\ 0\ 1\rangle T$ parallel to the barrel axis. There is a single activation energy for the onset of crystallization of 4.28×10^5 J mol^{-1}. The transformation kinetics fit the Johnson–Mehl–Avrami equation with an exponent of 4.

Acknowledgements

This work forms part of a research programme on metallic glasses supported by the Science Research Council and the Office of Naval Research (Contract no. N-00014-78-G-0048). We are grateful to JEOL (UK) Ltd for the use of STEM facilities. We acknowledge with pleasure the useful discussions with Professor R. W. Cahn, Dr B. Cantor, Dr S. Banerjee and other members of the Sussex Metastable Alloys Group.

References

1. W. KLEMENT, R. H. WILLENS and P. DUWEZ, *Nature* 187 (1960) 869.
2. "Metallic Glasses", ASM Seminar Series (ASM, Ohio, 1978).
3. "Rapidly Quenched Metals III", Proceedings of the 3rd International Conference on Rapidly Quenched Metals, Brighton 2–7 July 1978 (The Metals Society, London, 1978).
4. M. G. SCOTT, *ibid*, Vol. I, p. 198.
5. H. S. CHEN, *J. Appl. Phys.* 49 (1978) 3289.
6. T. EGAMI, *Mat. Res. Bull.* 13 (1978) 557.
7. H. H. LIEBERMANN, C. D. GRAHAM and P. J. FLANDERS, *I.E.E.E. Trans. Mag.* MAG 13 (1977) 1541.
8. C. D. GRAHAM, T. EGAMI, R. S. WILLIAMS and Y. TAKEI, *AIP Conf. Proc.* 29 (1976) 218.
9. F. E. LUBORSKY and J. L. WALTER, *J. Appl. Phys.* 47 (1976) 3648.
10. M. G. SCOTT, *J. Mater. Sci.* 13 (1978) 291.
11. F. E. LUBORSKY, *Mater. Sci. Eng.* 28 (1977) 139.
12. C. ANTONIONE, L. BATTEXXATI, A. LUCCI, G. RIONTINO and G. VENTURELLO, *Scripta Met.* 12 (1978) 1011.

13. J. L. WALTER, S. F. BARTRAM and R. R. RUSSELL, *Met. Trans.* 9A (1978) 803.
14. D. G. AST and D. KRENITSKY, *Mater. Sci. Eng.* 23 (1976) 241.
15. U. HEROLD and U. KOSTER, "Rapidly Quenched Metals III", Proceedings of the 3rd International Conference, Brighton, 2–7 July 1978 (The Metals Society, London, 1978) p. 281.
16. J. BURKE, "Kinetics of Phase Transformations in Metals" (Pergamon, Oxford, 1965) p. 192.
17. J. W. CHRISTIAN, "The Theory of Transformations in Metals and Alloys" (Pergamon, Oxford, 1965) p. 489.
18. W. B. PEARSON "Handbook of Lattice Spacings and Structures of Metals and Alloys" (Pergamon, Oxford, 1958).
19. U. KOSTER and U. HEROLD, *Scripta Met.* 12 (1978) 75.
20. P. G. BOSWELL and G. A. CHADWICK, *ibid* 10 (1976) 509.

Received 14 August and accepted 20 September 1979.